ELSEVIER

Implementation and evaluation of real-time model predictive control for load fluctuations mitigation in all-electric ship propulsion systems

Jun Hou[a], Ziyou Song[a,*], Hyeongjun Park[b], Heath Hofmann[a], Jing Sun[a,c]

[a] *Department of Electrical Engineering and Computer Science, University of Michigan, Ann Arbor, MI 48109, USA*
[b] *Department of Mechanical and Aerospace Engineering, New Mexico State University, Las Cruces, NM 88003, USA*
[c] *Department of Naval Architecture and Marine Engineering, University of Michigan, Ann Arbor, Michigan 48109, USA*

HIGHLIGHTS

- Real-time MPC has been implemented and evaluated in the physical testbed.
- Three special efforts are made to enable real-time implementation of MPC.
- Load fluctuations on the shipboard are addressed using real-time MPC.
- A filter-based algorithm is used to validate the effectiveness of MPC.
- The bus voltage variation and HESS loss can be reduced by up to 38% and 65%.

ARTICLE INFO

ABSTRACT

Electrification is a clear trend for both commercial and military ship development. Shipboard load fluctuations, such as propulsion-load fluctuations and pulse power loads, can significantly affect power system reliability. In order to address this issue, this paper explores a real-time model predictive control based energy management strategy for load fluctuation mitigation in all-electric ships. A battery combined with ultra-capacitor hybrid energy storage system (HESS) is used as a buffer to compensate load fluctuations from the shipboard network. In order to implement the proposed real-time MPC-based energy management strategy on a physical testbed, three special efforts have been made to enable real-time implementation: a specially tailored problem formulation, an efficient optimization algorithm and a multi-core hardware implementation. Given the multi-frequency characteristics of load fluctuations, a filter-based power split strategy is developed as a baseline control to evaluate the proposed MPC. Compared to the filter-based strategy, the experimental results show that the proposed real-time MPC achieves superior performance in terms of enhanced system reliability, improved HESS efficiency, long self-sustained time, and extended battery life. The bus voltage variation and hybrid energy storage losses can be reduced by up to 38% and 65%, respectively.

1. Introduction

The global warming is an international issue, which requires a decrease of fuel consumption and green house gas emission in all types of ships [1]. To achieve this goal, the propulsion system efficiency is required to be improved [2]. Electric propulsion could optimize the operation of onboard generators and facilitate the use of renewable energy sources and fuel cells [3]. Electric propulsion in marine applications is not a new concept, dating back over 100 years [4]. Marine electrification became increasingly popular after the development of high power

variable speed drives (VSDs) in the 1970's–1980's [5]. With the use of VSDs to electric propulsion motors, a common set of generators could power both the ship service and propulsion systems [6]. This concept is referred to as an integrated power system (IPS), which is the characterizing element of an all-electric ship (AES) [7].

IPS provides electrical power for both the propulsion system and service loads. Because of the integration of the shipboard network, load fluctuations from the propulsion system, as well as pulse-power loads from high-power missions, can significantly affect power quality and system reliability. In order to guarantee power quality and achieve

* Corresponding author.
E-mail addresses: junhou@umich.edu (J. Hou), ziyou@umich.edu (Z. Song), hjpark@nmsu.edu (H. Park), hofmann@umich.edu (H. Hofmann), jingsun@umich.edu (J. Sun).

Nomenclature

A_e/A_o	expanded blade-area ratio
C_{UC}	capacitance of ultra-capacitor
D_P	propeller diameter
$D_{1,2,...,4}$	duty cycle comments of DC/DC converters
I_B, I_{UC}	current of battery and ultra-capacitor
J_A, K_Q	advance and torque coefficients
N	predictive horizon
n, $Pitch/D_P$	propeller rotational speed and pitch ratio
P_B, P_{UC}	output power of battery and ultra-capacitor
P_{FL}	shipboard load power fluctuations
Q_B	capacity of battery
R_n	propeller Reynolds number
R_B, R_{UC}	internal resistance of battery and ultra-capacitor
S	sliding surface
SOC_B, SOC_{UC}	SOC of battery and ultra-capacitor
T_{load}	propeller torque
T_s	sampling time
V_{max}	maximum voltage of ultra-capacitor
V_{OC}	battery open circuit voltage
w	wake field
Z	number of propeller blades
β	loss factor
ρ	water density
AES	all-electric ship
AMPC	adaptive model predictive control
EMS	energy management strategy
ESS	energy storage system
HESS	hybrid energy storage system
IPA-SQP	integrated perturbation analysis and sequential quadratic programming
IPS	integrated power system
MPC	model predictive control
MPEL	Michigan Power and Energy Lab
PA	perturbation analysis
SQP	sequential quadratic programming
UC	ultra-capacitor
VSD	variable speed drive

superior reliability, effects of load fluctuations must be mitigated. Given the diverse characteristics of shipboard load fluctuations, such as those due to propulsion-load fluctuations [8] and on-and-off of pulse-power loads, energy storage systems (ESSs) and advanced control algorithms are required [9]. Using single type of ESS can result in increased size, weight, and cost for electric ship operations [10]. Different combinations of ESSs are also investigated in different applications [11–15]. In [11], the engine-generator, battery and ultracapacitor (UC) are explored for a plug-in hybrid electric vehicle (PHEV). The literature [12] uses battery with UC to improve the efficiency and durability of a PHEV. In [13], different control strategies of battery combined with UC for an electric city bus have been studied. The benefits of using UC to improve the battery life cycle in a low temperature are further explored in [14]. The ZEBRA batteries with UC in a commercial vehicle have been studied in [15], and the experimental results demonstrate the benefits of this combination of ESSs. In this paper, hybrid energy storage systems (HESSs), where batteries and ultra-capacitors are used as a buffer to mitigate shipboard load fluctuations [16], are investigated. The lithium-ion batteries are chosen due to their higher power and energy densities [17].

IPS with HESS are expected to manage multiple objectives, including improving fuel efficiency, enhancing response speed, and strengthening reliability [18]. Advanced optimization-based energy management strategies are essential to achieve desired trade-off among these competing objectives [19]. Model predictive control (MPC) is an effective optimization-based approach [20]. Compared to LQG, MPC does not require unique performance criteria, and it is able to deal with constraints and process nonlinearities [21]. MPC has been successfully implemented in process industries. Recently, MPC becomes one of the promising control strategy in many applications, such as micro-grids [22], (hybrid) electric ships [23], and (hybrid) electric vehicles [24]. The sampling periods in most of those applications are from seconds to hours. However, the sampling period in this study is on the order of milliseconds, which makes the MPC implementation more difficult. In order to implement real-time MPC, the explicit MPC is one solution, which uses offline computations to reduce the computational time [25]. Online linearization is another popular approach to enable real-time feasibility [26]. Typically, the quadratic programming (QP) formulation is preferred to solve the optimization problem efficiently [27]. However, the problem studied in this paper is nonlinear and non-convex, which requires advanced optimization solver.

In marine applications, MPC can exploit the optimal solution with a receding horizon to address constraints, such as physical dynamics and operation boundaries of IPS and HESS [28]. MPC is therefore used in this paper as an optimization-based energy management strategy (EMS). In [29], a nonlinear MPC is developed to compensate the pulse power load and follow the desired references, including the desired bus voltage, reference power for generator sets and reference speed for the motor. A sensitivity-function-based approach is proposed in [30] in order to achieve real-time trajectory tracking. In [31], the stochastic MPC is developed to smooth out low-frequency power fluctuations. Scenario-based MPC is developed for dynamic safety constraints in [32]. Multi-level MPC is used in [33] to address the disturbances from the environment. However, most of those state-of-the-art MPC-based EMSs only present software or hardware-in-the-loop simulation results. The main challenge to implement the MPC-based approaches is to solve the optimization problem in real-time within a relatively short sampling period, as the system dynamics in this paper is fast and the sampling period is on the order of milliseconds.

The objective of this paper is to address shipboard load fluctuations, including not only propulsion-load fluctuations but also pulse-power loads, and validate the effectiveness of MPC on a physical testbed. A filter-based power split EMS is used as a baseline strategy to illustrate the benefits of the proposed MPC-based EMS. For the filter-based EMS, the battery compensates low-frequency load fluctuations, while the UC handles high-frequency fluctuations. Note that the filter-based EMS requires much less computational time, which makes it easy to implement in real time. On the other hand, the main challenge for MPC based EMS is to handle the computational tasks. In order to achieve real-time feasibility of the proposed MPC-based EMS, three special efforts have been made:

- A novel MPC formulation with state of charge (SOC) reference being incorporated is used to achieve the desired performance with a relatively short predictive horizon [16].
- An integrated perturbation analysis and sequential quadratic programming (IPA-SQP) algorithm [34] is used to solve the optimization problem with high computational efficiency.
- A multi-core hardware implementation is used for the real-time system controller to guarantee system signal synchronization and separate system-level and component-level controls, thereby increasing real-time capabilities.

Load fluctuation compensation and HESS loss minimization are two main control objectives for the load fluctuation mitigation problem. In order to implement MPC in real-time, a short predictive horizon is

preferred. However, the short-horizon MPC cannot incorporate the long-term perspectives of operation. Due to the smaller internal resistance of UC, the UC will be tasked to compensate the load fluctuations as much as possible, leading to a rapid decreasing in its SOC. As the UC SOC decreases, delivering the same output power requires a larger current and results in significantly increased losses. In this paper, an SOC reference of UC is incorporated in the MPC optimization problem formulation to address the limitations imposed by short predictive horizons.

To solve the optimization problem efficiently, we use IPA-SQP approach. The IPA-SQP approach, developed for nonlinear MPC in [35], combines solution updates derived using perturbation analysis (PA) and sequential quadratic programming (SQP). For the PA-based update, IPA-SQP exploits neighboring extremal (NE) optimal control theory extended to discrete-time systems with constraints [36] to improve computational efficiency. The solution at time t is obtained as a correction to the solution at time $(t-1)$ through the NE update. If the NE update is not fulfilling optimality criteria, one or multiple SQP updates are used until the optimality criteria are satisfied. The merged PA and SQP updates yield a fast solver for NMPC problems [37].

In order to provide a physical platform for shipboard EMS experimental validations, a physical test-bed has been constructed in the University of Michigan Power and Energy Lab (MPEL). This state-of-the-art test-bed consists of a system controller, electric machines, high-power converters, energy storage devices (batteries, UCs, and flywheel) and a high-power load resistor bank. The system controller has multiple cores which can be used to separate the system-level MPC-based EMS and component-level controls, and therefore increases its real-time capability.

In our previous work, the modeling of propulsion-load fluctuations has been developed [16]. Furthermore, compared to the single type of ESS, the advantages of HESS have been discussed, and the MPC algorithm used in this paper has been proposed and investigated with a simulation study. However, uncertainties were not taken into consideration in [16], which makes the control solution impossible to be directly used in the experiments. In order to deal with uncertainties and enable real-time implementation, the bus voltage regulation is combined with the real-time MPC, and this combination has been successfully implemented in the physical testbed. The work in [8] mainly provides insights into the comparison between batteries/flywheels and batteries/UCs. This paper focuses on the implementation and evaluation of the proposed real-time MPC. The novelties and contributions of this paper are summarized in the following:

1. This paper not only addresses the propulsion-load fluctuations, but also takes the pulse-power load into consideration, which makes this study closer to real applications. Furthermore, it also demonstrates that the proposed method could deal with more general load fluctuation problems, such as load fluctuations in electric vehicles or shore-based microgrids.
2. The implementation and evaluation of the real-time MPC is the main contribution of this paper. Three special efforts have been made to enable real-time implementation: a specially tailored problem formulation, an efficient optimization algorithm and a multi-core hardware implementation. These efforts can be used for other applications as well. Furthermore, in order to deal with the uncertainties in the experiments, the voltage regulator is also integrated.

The paper is organized as follows. In Section 2, the shipboard load fluctuation problem and control objectives are described, and the optimization-oriented model is presented. A specially tailored MPC-based EMS is developed as a system-level controller, and the IPA-SQP algorithm is introduced. The component-level controllers, such as the current regulators for HESS, are developed in Section 3. In Section 4, the multi-core implementation is performed and the experimental results
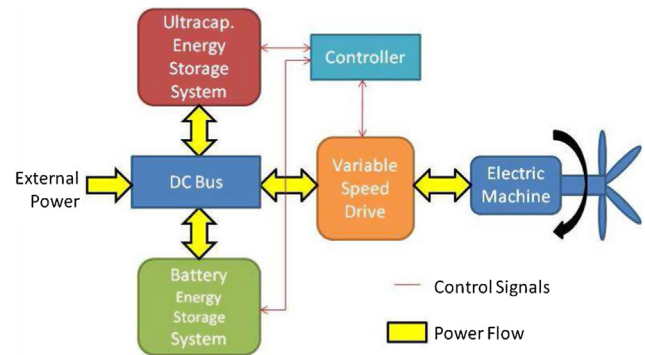

Fig. 1. Schematic diagram of electric drive system with hybrid energy storage [16].

on the physical test bed are presented and analyzed. Compared to the filter-based EMS, the proposed MPC-based EMS achieves superior performance in terms of reduced bus voltage variations, reduced battery peak and RMS currents, and reduced HESS losses. Section 5 concludes the paper.

2. System-level controller development: energy management strategy

2.1. Control objectives

The system concept is shown in Fig. 1, where the HESS serves as a buffer to isolate the power network from the propulsion load fluctuations. We assume the motor is working at the nominal operating point and the generator sets provide the average power.

In DC shipboard networks, the variation of the DC bus voltage reflects the power quality and the stability of the DC ship power system [38]. Therefore, the first control objective of the power management system is guaranteeing power quality and system reliability, which translates into DC bus voltage stability.

The second control objective is to optimize system efficiency. In order to improve the system efficiency, the losses of HESS must be minimized and the sensitivity of power losses to HESS operating condition needs to be exploited. Furthermore, a long self-sustained operation time (i.e., the operation time before the HESS will be charged by or discharged to external power sources) is preferred, which implies that we should take advantage of the battery's high energy density [16].

The third control objective is to extend battery life. Batteries aging is accompanied by its capacity decrease [39] and its resistance increase [40]. Numerous publications have associated the battery C-rate operation and usage with the battery life cycle [41]. In this paper, the battery peak and RMS currents are used to represent high C-rate operation and battery usage.

The control objectives considered in this paper for HESS power management development are therefore summarized as follows.

- Assure system reliability: compensate load fluctuations and maintain the DC bus voltage at the desired value.
- Optimize system efficiency: minimize HESS losses.
- Extend battery life cycle: reduce battery peak and RMS currents.

2.2. Hybrid energy storage system model

For the HESS model, we define the states as the state of charge (SOC) of the batteries (SOC_B) and ultra-capacitor (SOC_{UC}), and the control variables as the battery current (I_B) and the ultra-capacitor (I_{UC}):

$$x = \begin{bmatrix} x_1 \\ x_2 \end{bmatrix} = \begin{bmatrix} SOC_B \\ SOC_{UC} \end{bmatrix}, \quad u = \begin{bmatrix} u_1 \\ u_2 \end{bmatrix} = \begin{bmatrix} I_B \\ I_{UC} \end{bmatrix}, \qquad (1)$$

where the SOC of the battery is defined $SOC_B = \frac{Q_{battery}}{Q_B} \times 100\%$, where $Q_{battery}$ and Q_B in Ampere-hour are the current and maximum capacity of the battery, respectively; the SOC of the ultra-capacitor is defined as $SOC_{UC} = \frac{V_{UC}}{V_{max}} \times 100\%$, where V_{UC} and V_{max} are the voltage and maximum voltage of ultra-capacitors. The HESS model is presented as follows:

$$\dot{x}_1 = \frac{-u_1}{3600 Q_B},$$
$$\dot{x}_2 = \frac{-u_2}{V_{max} C_{UC}}, \qquad (2)$$

where C_{UC} is the capacitance of the ultra-capacitor. The terminal powers of the HESS are obtained as follows:

$$P_B = V_{OC} u_1 - R_B u_1^2,$$
$$P_{UC} = V_{max} x_2 u_2 - R_{UC} u_2^2, \qquad (3)$$

where V_{OC} and R_B are the open-circuit voltage and internal resistance of the battery; and R_{UC} is the internal resistance of the ultra-capacitor. In this paper, the internal resistance model is used to evaluate the HESS power loss. In the literature, there are considerable models of battery and ultracapacitor. For example, the first-order equivalent circuit model (an internal resistance with a parallel RC network) is one of effective battery models [42], and it has been widely used in many applications, such as the system level energy management strategy development [43]. However, according to our parameter identification results, the RC time constant of the battery pack in our testbed is about 60 s, which is much higher than the sample time of the MPC (0.01 s). Therefore, this RC pair has slight impact on the MPC performance. Furthermore, the parallel RC network will introduce another state into MPC, leading to increased computational cost. As a result, the control-oriented HESS model with only one internal resistance is used in this paper.

2.3. Energy management strategy

Filter-based control strategies [44] and independent PI voltage regulators [45] have been investigated for HESS in marine applications. The filter-based control splits the load power into high-frequency and low-frequency components, then use UC to deal with the high-frequency components and battery to address the low-frequency components. The drawback of independent PI bus voltage regulators for multiple energy sources is lack of coordination and therefore negative impact on performance. In [46], experimental results show that the filter-based control strategy outperforms the independent PI control strategy. In this paper, the filter-based power split control strategy is used as a baseline control to evaluate the effectiveness of the proposed

real-time MPC strategy. The schematic of the filter-based controller is shown in Fig. 2, where a low-pass filter is used to create the power split, and a voltage regulator using UC is used to deal with disturbance and uncertainties. In order to perform a fair comparison, the same voltage regulator is used in the real-time MPC. The schematic of the real-time MPC is shown in Fig. 3. In order to achieve the control objectives discussed in the previous section, the optimization problem is formulated as follows. Minimize the following cost function with the predictive horizon N:

$$\begin{aligned} J_{HESS}(x(k), u(k)) = &\sum_{k=t}^{t+N} (1-\lambda)(P_{FL}(k) - P_B(k) - P_{UC}(k))^2 \\ &+ \lambda(R_B u_1^2(k) + R_{UC} u_2^2(k)) \\ &+ \gamma_{UC_{SOC}} (x_2(k) - SOC_{UC_{ref}})^2, \end{aligned} \qquad (4)$$

subject to the constraints:

$$\begin{aligned} 20\% &\leqslant x_1 \leqslant 90\%, \\ 50\% &\leqslant x_2 \leqslant 99\%, \\ -30A &\leqslant u_1 \leqslant 30A, \\ -30A &\leqslant u_2 \leqslant 30A, \end{aligned} \qquad (5)$$

$$\begin{bmatrix} x_1(k+1) \\ x_2(k+1) \end{bmatrix} = \begin{bmatrix} 1 & 0 \\ 0 & 1 \end{bmatrix} \begin{bmatrix} x_1(k) \\ x_2(k) \end{bmatrix} - \begin{bmatrix} \frac{T_s}{3600 Q_B} & 0 \\ 0 & \frac{T_s}{V_{max} C_{UC}} \end{bmatrix} \begin{bmatrix} u_1(k) \\ u_2(k) \end{bmatrix}. \qquad (6)$$

Because of the smaller internal resistance of UC, minimizing the HESS losses term $(R_B u_B^2(k) + R_{UC} u_{UC}^2(k))$ can also reduce the battery RMS and peak currents. There is an additional SOC reference term $((x_2(k) - SOC_{UC_{ref}})^2)$ in the cost function, which aims to address the limitation of a short predictive horizon. For example, without the SOC penalty of UC, the short-horizon MPC is not able to maintain the UC operating in its high SOC range, because the benefit of maintaining it is too small in the short term and is therefore ignored in the optimization [16]. As a result, the SOC of the UC drops quickly. As it decreases, the delivery of the same output power requires a larger current, thereby leading to significantly increased losses and power tracking error. With the SOC penalty, the UC maintains its operation in a high SOC range. The SOC reference term ($\gamma_{UC_{SOC}} (x_2(k) - SOC_{UC_{ref}})^2$) has been demonstrated to be important to MPC performance [16]. The value of $\gamma_{UC_{SOC}}$ depends on the sea state, and it is determined by the offline simulations, as shown in Fig. 4. Since the higher SOC of UC is preferred in terms of its efficiency and maximum power capability, the $SOC_{UC_{ref}}$ is designed to be close to its upper boundary (99%). Note that $SOC_{UC_{ref}}$ cannot be 99%, because UC is required to absorb energy as well.

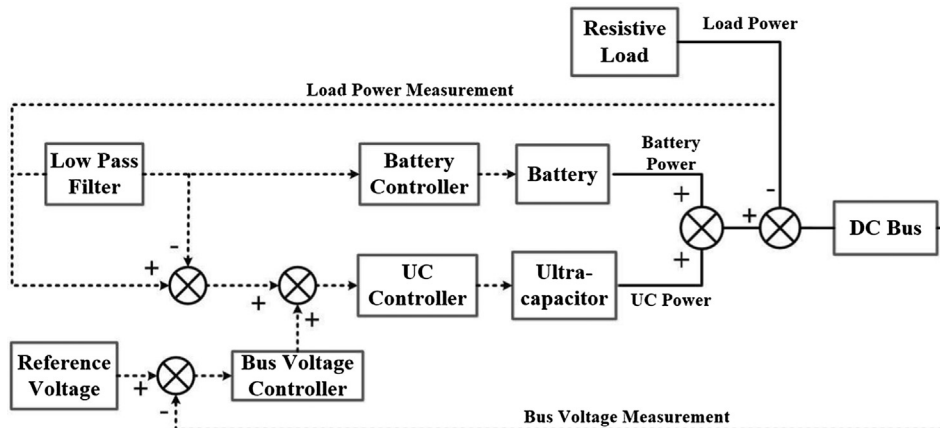The IPA-SQP algorithm, which includes prediction-correction in

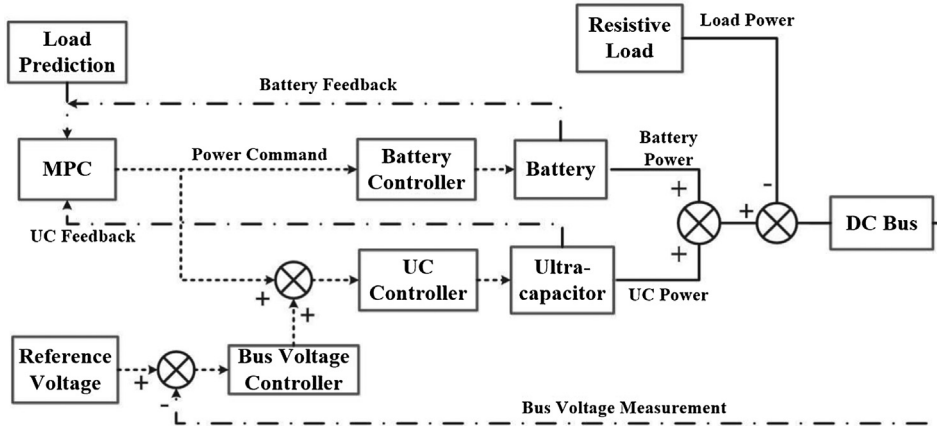Fig. 2. Schematic of the filter-based power split control.

Fig. 3. Schematic of the real-time MPC.

approximating the optimal solution numerically, is used to solve the optimization problem efficiently. IPA-SQP uses neighboring extremal (NE) updates in the prediction step to improve computational efficiency [34]. The IPA-SQP approach combines the solutions derived using PA and SQP. This approach updates the solution to the optimization problem at time t by considering it as a perturbation to the solution at time $(t-1)$ using neighboring optimal control theory [36] extended to discrete-time systems with constraints, and then corrects the results using SQP updates. The merged PA and SQP updates exploit the sequential form of predictor-and-corrector steps and closed-form solution of PA, thereby yielding a fast solver for nonlinear MPC problems [37]. The flowchart of IPA-SQP is shown in Fig. 5 [47], which illustrates the main steps of the IPA-SQP algorithm obtain the NE solutions and to deal with changes in the activity status of constraints.

3. Electric propulsion drive testbed and component-level control

In order to provide a flexible hardware environment for the testing and validation of control algorithms for electric propulsion systems with HESS, the Advanced Electric Drive with AED-HES test-bed has been constructed in the Michigan Power and Energy Lab. The test-bed photo is shown in Fig. 6. In the test-bed, the power electronic converters, which serve as actuators in directing the power flow to and from various components of the test-bed, are controlled by a central micro-controller (Speedgoat). Since there is no generator in our testbed, we use a DC/DC converter to provide the average power to the DC bus in order to emulate impacts of generator sets.

A Lithium-Iron-Phosphate battery chemistry has been selected for its high energy density and superior thermal and chemical stability. Currently, the battery consists of four 38.4 V, 100 A h modules, as
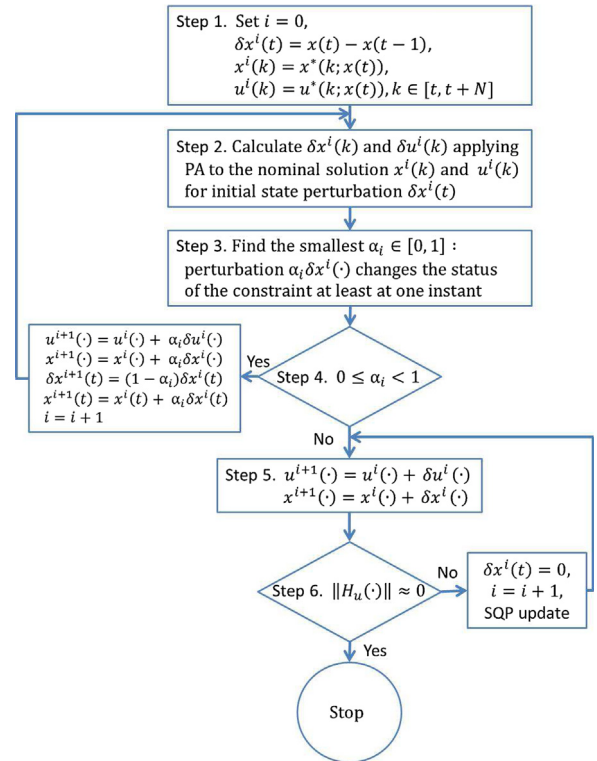
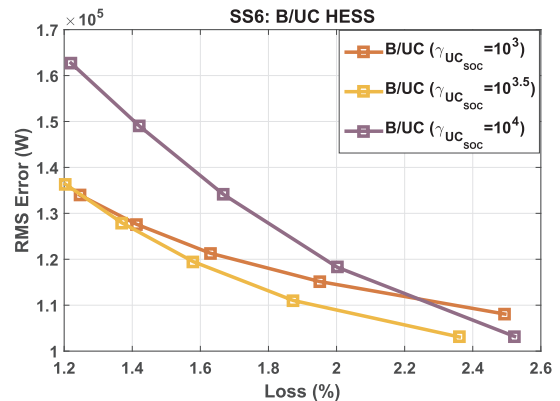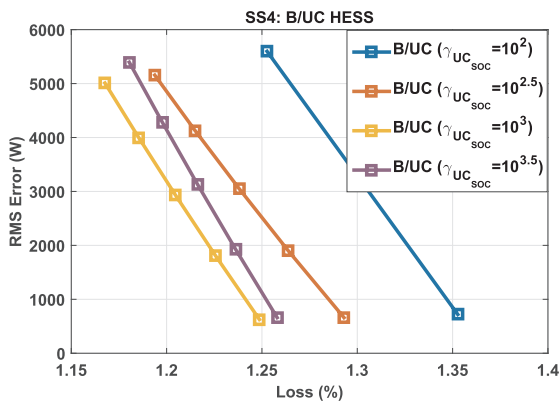

Fig. 5. Flowchart of the IPA-SQP algorithm [47].

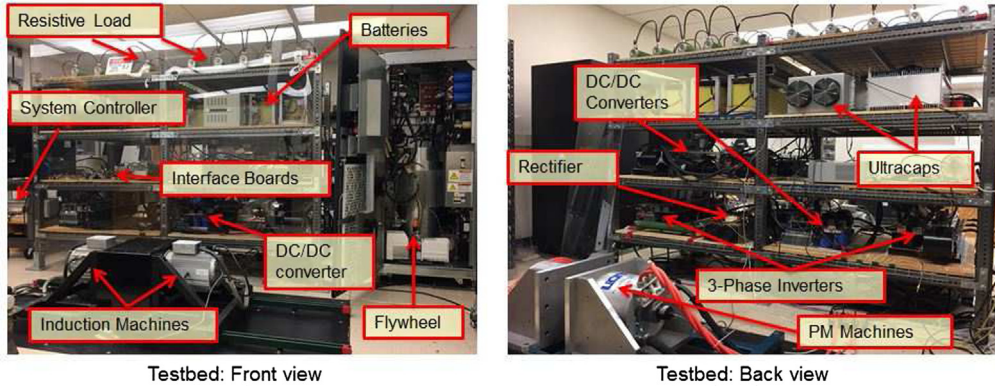**Fig. 4.** Pareto-front of B/UC HESS at sea state 4 (left) and sea state 6 (right) with different $\gamma_{UC_{SOC}}$.

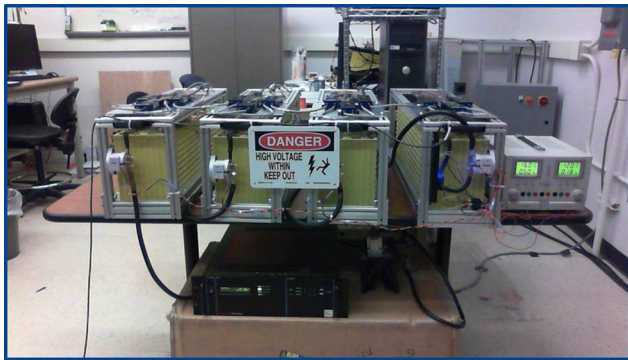**Fig. 6.** MPEL AED-HES test-bed.

Fig. 7. Battery module of MPEL test-bed.

Table 1
Specifications for the battery system.

Li-ION battery	
Manufacturer:	Flux Power®(BMS) & Winston®(cells)
Voltage limits (max/min):	3.9 V/2.5 V
Max. continuous current:	3C
Capacity:	100 A h
DC voltage:	36–154 V (in 38.4 V increments)
Communication Interface:	CAN bus

Fig. 8. UC module of MPEL test-bed.

Table 2
Specifications for the ultra-capacitors.

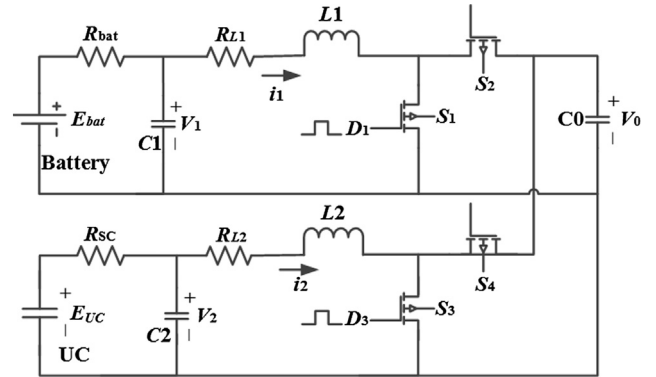| Ultra-capacitor	
Manufacturer:	Maxwell Technologies®
Rated capacitance:	63 F
Rated voltage:	125 V
Max. continuous current:	240 A at 40 °C
Max. equivalent series resistance:	18 m Ω

Fig. 9. Circuit diagram of bi-directional DC/DC converters for HESS.

shown in Fig. 7, which can be connected in series to provide a pack voltage of up to 154 V. The nominal cell voltage is 3.2 V. The individual cells have bolted interconnections via copper bus bar, and a Battery Management System (BMS) from Flux Power®utilizes a distributed architecture, where every BMS module manages 4 cells via passive (resistive shunting) cell balancing. The Battery Control Module (BCM) measures battery current to compute the SOC of the pack in addition to monitoring cell voltages and thermal feedback from the individual BMS's via a CANbus network. In the event of a problem (over/under-voltage cell or over-temperature cell), the BCM will open contactor relays to prevent damage to the battery system (see Table 1).

The test-bed has four 63 farad/ 125 volt ultra-capacitors from Maxwell Technologies®, as shown in Fig. 8, which can be connected in series/parallel combinations to suit testing needs. The modules provide analog feedback measurements of temperature and voltage, and interface with the DC bus via a current-regulated power electronic converter. Manufacturer specifications for the ultra-capacitors are provided in Table 2. In this experiment, two ultra-capacitors are used and connected in series.

In this testbed, bi-directional DC/DC converters are used for HESS control. The circuit diagram of the bi-directional DC/DC converters is shown in Fig. 9. The average-value model of the HESS can be described as follows:

$$\dot{V}_1 = -\frac{V_1 + i_1 R_{bat} - E_{bat}}{C_1 R_{bat}},$$
$$\dot{V}_2 = -\frac{V_2 + i_2 R_{UC} - E_{UC}}{C_2 R_{UC}},$$
$$\dot{i}_1 = \frac{V_1 - i_1(R_{L1} + R_{on2}) - V_0 + D_1[i_1(R_{on2} - R_{on1}) + V_0]}{L_1},$$
$$\dot{i}_2 = \frac{V_2 - i_2(R_{L2} + R_{on4}) - V_0 + D_3[i_2(R_{on4} - R_{on3}) + V_0]}{L_2},$$
$$\dot{V}_0 = \frac{i_1 + i_2 - i_{load} - D_1 i_1 - D_3 i_2}{C_0},$$

(7)

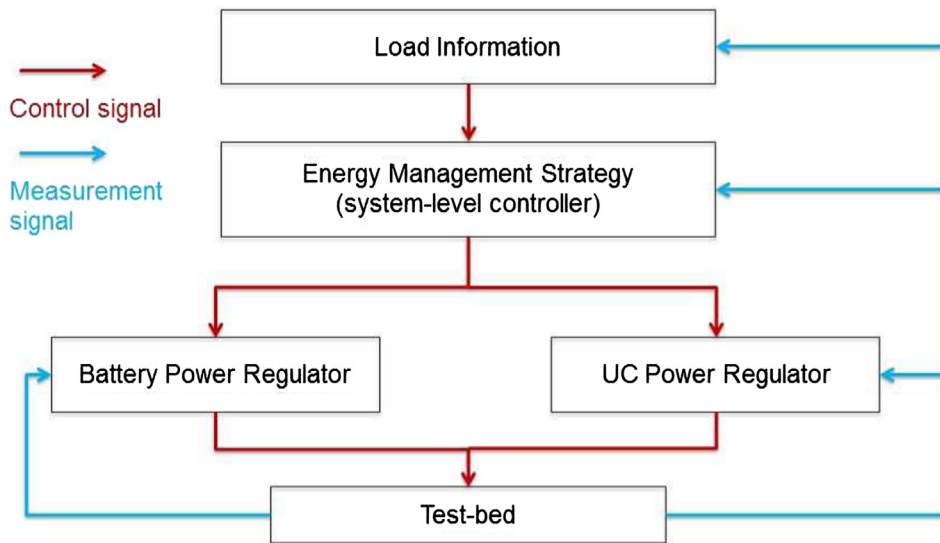where C_0 is the bus capacitor; C_1, and C_2 are the capacitors in parallel

Fig. 10. Hierarchical control structure for real-time control implementation.

Table 3
Parameters for simulation study.

| Description	Parameter	Value
Ship length	L_{ship}	190 m
Ship breadth	B_{ship}	28.4 m
Draft	H	15.8 m
Mass	m	20,000 ton
Added-mass	m_x	28,755 ton
Thrust deduction coefficient	t_d	0.2
Propeller diameter	D	5.6 m
Wetted area	S	12,297 m^2
Advance facing area in the air	A_T	675.2 m^2
Water resistance coefficients	$C_F + C_R$	0.0043
Air resistance coefficient	C_{air}	0.8
Wave period	T_{wave}	12 sec
Wave height	h_{wave}	2 m(SS4)/ 4 m(SS6)
Wave length	L_{wave}	40.29%L_{ship}
Ship speed command	U_d	12.4 knot
Motor speed command	ω_d	125 rpm
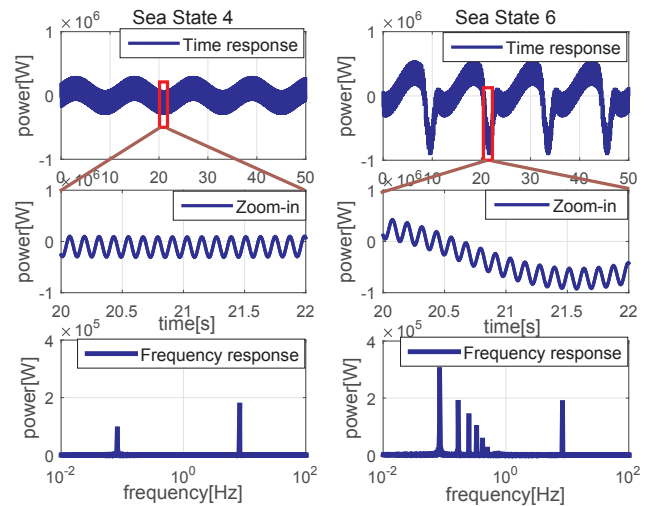
Fig. 12. Load power fluctuations (top plots), zoom-in fluctuations (middle plots), and their frequency spectrums (bottom plots) [16].
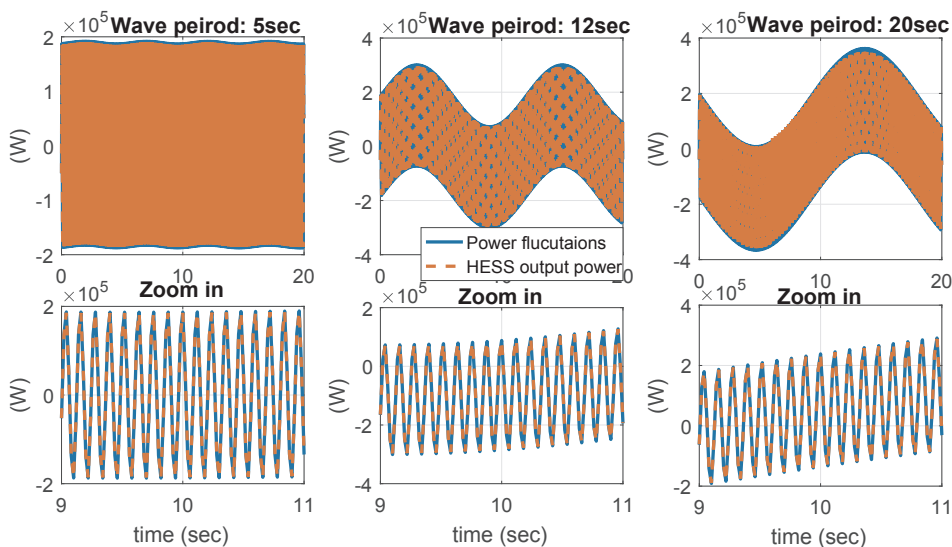

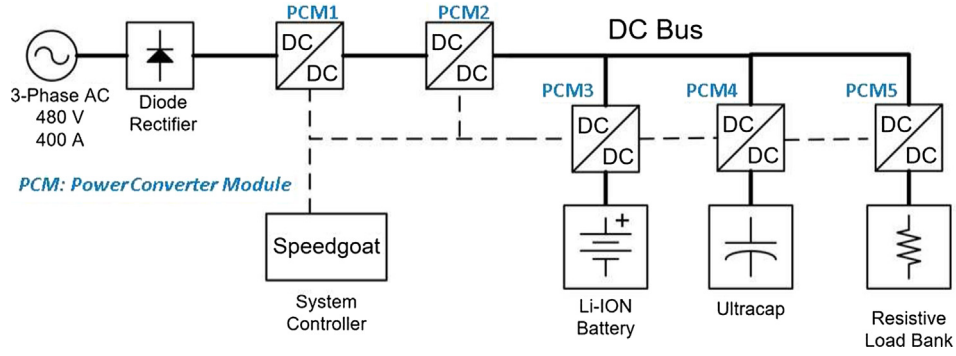**Fig. 11.** HESS power tracking performance with different wave periods.

Fig. 13. Diagram of real-time MPC experiment.

Table 4
Manufacturer specifications for system controller.

System controller	
Manufacturer:	Speedgoat®
Processor:	Intel Core i5-680 3.6 GHz
Main drive:	320 GB SATA Hard Disk
Memory:	DDR3 4096 MB
Serial ports:	4 × RS232
Software:	Simulink Real-Time®
PWM outputs:	18
Quadrature decoding inputs:	2
Digital inputs/outputs:	4
Analog-to-digital inputs:	16 in differential mode
Controller area network (CAN):	1
Ethernet communication block:	1

with the battery and UC, respectively; V_0, V_1 and V_2 are the voltages corresponding to capacitors C_0, C_1, and C_2, respectively; L_1, and L_2 are the inductors of the bi-directional DC/DC converters; i_1 and i_2 are the inductor currents; R_{L1}, and R_{L2} are the resistance of inductor L_1 and $L2$, respectively; and D_1 and D_3 are the duty cycle commands of the DC/DC converters.

The hierarchical control structure is shown in Fig. 10. To implement the system-level EMS, component-level controllers are required to follow the reference power commands. As shown in Eq. (7), the HESS with bi-directional converters model is nonlinear, and its control requires a robust nonlinear approach. Sliding-mode control is a natural candidate, which has been successfully applied to robot manipulators, vehicles, high-performance electric motors, and power systems [48]. In this paper, the sliding-mode control presented in [49] is used to control the bi-directional DC/DC converters. The sliding surface is defined as $S = [S_1, S_2]^T$, where $S_1 = i_{1ref} - i_1$ and $S_2 = i_{2ref} - i_2$.

In order to ensure the existence of the sliding-mode surface, the condition $\dot{S}S < 0$ must be satisfied. The differential sliding variable is set as:

$$\dot{S} = -KS - \varepsilon sat(S), \tag{8}$$

where the saturation function $sat(S)$ is defined as:

$$sat(S_n) = \begin{cases} 1, & S_n \in (1, \infty), \\ S_n, & S_n \in [-1, 1], \\ -1, & S_n \in (-\infty, -1), \end{cases} \tag{9}$$

and $n = 1$, 2, K and ε are the sliding-mode gains.

To simplify the solution, we assume that $R_{on1} = R_{on2}$ and $R_{on3} = R_{on4}$. Assuming a time scale separation (i.e., the current dynamic is much faster than the voltage dynamic, the voltages $V_{0,1,2}$ are assumed to be constant. Therefore, the sliding-mode control law is developed as follows [49]:

$$\begin{bmatrix} D_1 \\ D_3 \end{bmatrix} = \begin{bmatrix} 1 - \frac{V_1}{V_0} + i_1 \frac{R_{L1} + R_{on2}}{V_0} + K_1 \frac{L_1}{V_0}(i_{bat,ref} - i_1) + \varepsilon_1 \frac{L_1}{V_0} sat(i_{bat,ref} - i_1) \\ 1 - \frac{V_2}{V_0} + i_2 \frac{R_{L2} + R_{on4}}{V_0} + K_2 \frac{L_2}{V_0}(i_{UC,ref} - i_2) + \varepsilon_2 \frac{L_2}{V_0} sat(i_{UC,ref} - i_2) \end{bmatrix}. \tag{10}$$

4. Experimental implementation and performance evaluation

In this section, the experimental setup is introduced at the beginning. And then, the component-level controllers are validated that the HESS can accurately follow the power command. After that, the real-time simulation of both the system-level and component-level controllers is performed to validate the computational capability. The experimental results are presented and discussed at the end.

4.1. Propeller and ship dynamic model

In order to capture the dynamics of the load fluctuations and the HESS, a control-oriented model of an electric ship propulsion system with HESS is presented. The key elements of the model are presented in this section for easy reference, and the detailed description of the model can be found in [16]. A cargo ship is studied in this paper, and its
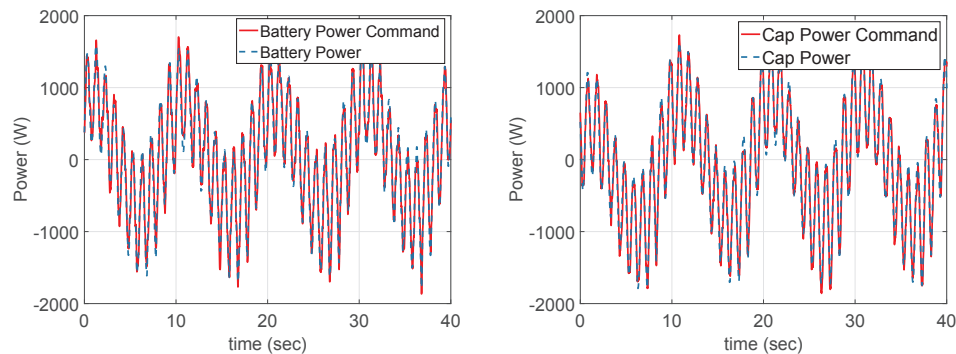

Fig. 14. Control performance: battery and UC command power and actual power.
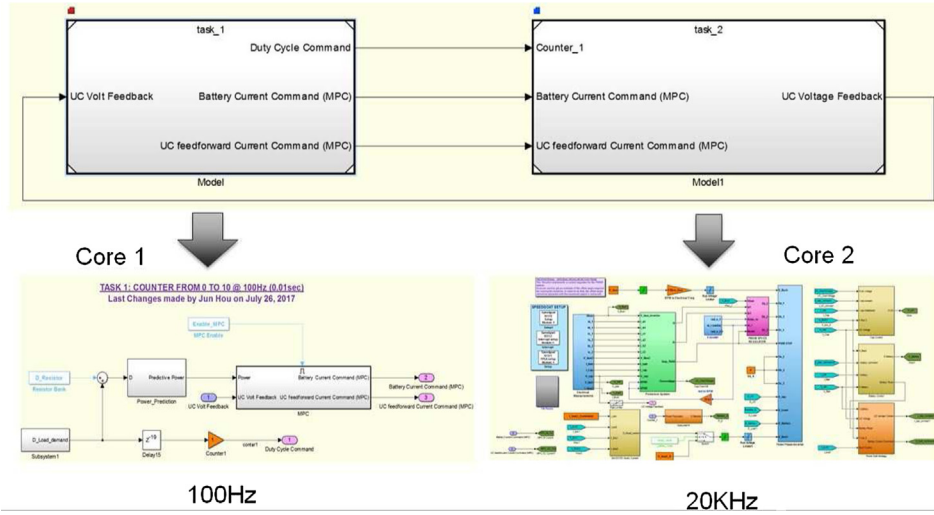
Fig. 15. Multi-core structure of Speedgoat.

Fig. 16. Real-time simulation evaluation of system-level controller (core1).

Fig. 17. Real-time simulation evaluation of component-level controllers (core2).

parameters as well as the parameters associated with wave behaviors and operating conditions are listed in Table 3. The periods of ocean waves are typically from 4 s to 12 s [50]. Because of the large ship mass $(m + m_x)$, the impact of the high-frequency wave on the shipboard network, e.g., 5 s, will be significantly reduced. As shown in Fig. 11, the amplitude of 5-s wave is much smaller than the other two. Since we would like to study the worst-case scenario in the common condition (4–12 s), we choose 12 s in this manuscript. Fig. 11 also demonstrates the effectiveness of the proposed solution with different wave periods.

The propeller and ship model captures the dynamic behavior of the propeller and ship motion, and determines the load power fluctuations (P_{FL}), which is the power demand of HESS. The mechanical load power transmitted to the ship body from the propeller can be expressed as:

$$P_{Load} = 2\pi n T_{Load},$$ (11)

where T_{Load} is the propeller torque and n is the rotational speed of the propeller in revolutions-per-second. The propeller is assumed to be directly connected to the motor (as typically done for all-electric ships), so n is also the rotational speed of the motor. The torque generated by the propeller can be expressed as:

$$T_{Load} = \text{sgn}(n)\beta K_{Q0}\rho n^2 D_P^5,$$ (12)

where K_{Q0} denotes the torque coefficient when no losses are present, β is the loss factor which is used to capture the effects of in-and-out water motion of the propeller, ρ is the density of water, and D_P is the diameter of the propeller. The torque coefficient is determined as follows:

$$K_{Q0} = f_{K_Q}(J_A, Pitch/D_P, A_e/A_o, Z, R_n),$$ (13)

where $J_A = \frac{V_a}{nD_P}$ is the advance coefficient with V_a being the ship advance speed, $Pitch/D_P$ is the pitch ratio, A_e/A_0 is the expanded blade-area ratio, Z is the number of blades, and R_n is the Reynolds number. Note that the wake field, defined as $w = \frac{U - V_a}{U}$, should be taken into account, which includes the average and fluctuation components.

Note that the high-frequency fluctuations are mainly caused by the variations of wake field in w and the low-frequency fluctuations are caused by the wave effect through the ship speed U and the in-and-out of water loss factor β. In this paper, a high-gain speed control is used to study the worst-case scenario, namely the load torque balanced by the motor torque. As discussed in [51], the torque or power control, especially power control, could reduce the torque or power fluctuations on the shipboard network. However, they are more suitable at nominal sea states, where the propeller is always in the water. If the propeller is in-and-out of water, the good properties of torque and power control will turn to the opposite.

The power load fluctuations of a cargo ship in both the time and frequency domains are shown in Fig. 12 [16], where the responses in two sea states (sea state 4 and sea state 6) are shown side-by-side. Sea state 4 represents a moderate sea condition and is considered as the nominal condition. Sea state 6 represents a rough sea condition, where the propeller can be in-and-out of water. The load power fluctuation (P_{FL}) shown in Fig. 12 is that the total load power (P_{Load}) minuses the propulsion power (the average value of P_{Load}). Positive fluctuations mean that the system is overload, so that the HESS should provide power (discharging), while negative fluctuations mean that the system is underload, then the HESS should absorb power (charging). The reason why large load power fluctuations appear at sea state 6 is that the propeller could be in-and-out of water.

In order to predict the propulsion-load fluctuations, a simplified model-based approach is used [52]. Since the prediction cannot be evaluated in this testbed, only the impact of the predictive horizon will be studied in the experiments. As the predictive horizon increases, more future information can be obtained, but the predictive error will be increased at the same time.
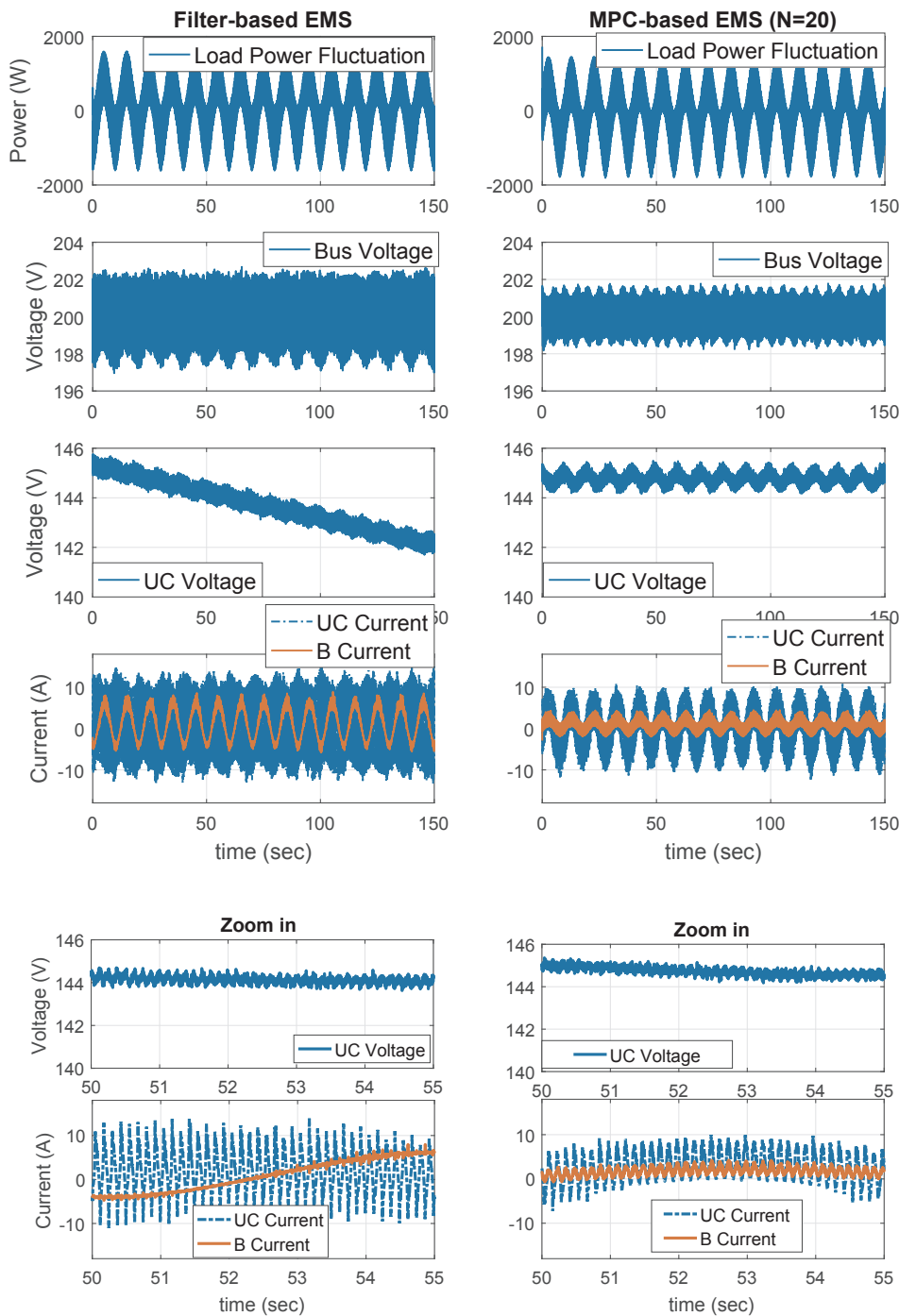
Fig. 18. Experimental results of sea state 4: MPC vs. filter-based control.

Table 5
Performance comparison: filter-based vs. MPC.

	SS4	SS6	SS4 with pulse
$Volt_{var}$	38.04%	36.05%	28.90%
$HESS_{Loss}$	65.95%	50.23%	64.18%
B_{Peak}	48.89%	32.65%	46.50%
B_{RMS}	59.01%	35.81%	49.64%

4.2. Experimental setup

In this experiment, the desired DC bus voltage is defined as 200 V, and the maximum voltage and the desired reference voltage of UC are defined as 150 V and 145 V, respectively. The maximum and minimum output currents of the battery and UC are 30 A and −30 A, respectively. Typically, the DC bus voltage of MVDC shipboard networks is constant, so that only a constant desired DC bus voltage is considered in this paper. The load fluctuations in Fig. 12 are scaled to a peak value of 2 kW. Uncertainties, such as load uncertainties, parameter uncertainties, modeling uncertainties, and measurement uncertainties, exist in the system and can be used to evaluate the robustness of the proposed controller. A diagram of this experimental setup is shown in Fig. 13. A three-phase diode rectifier converts the AC power from the grid to DC power, and then a DC/DC converter (PCM1) "bucks" the DC voltage down to the nominal voltage. We note that a constant duty cycle is used for this DC/DC converter. In order to emulate the
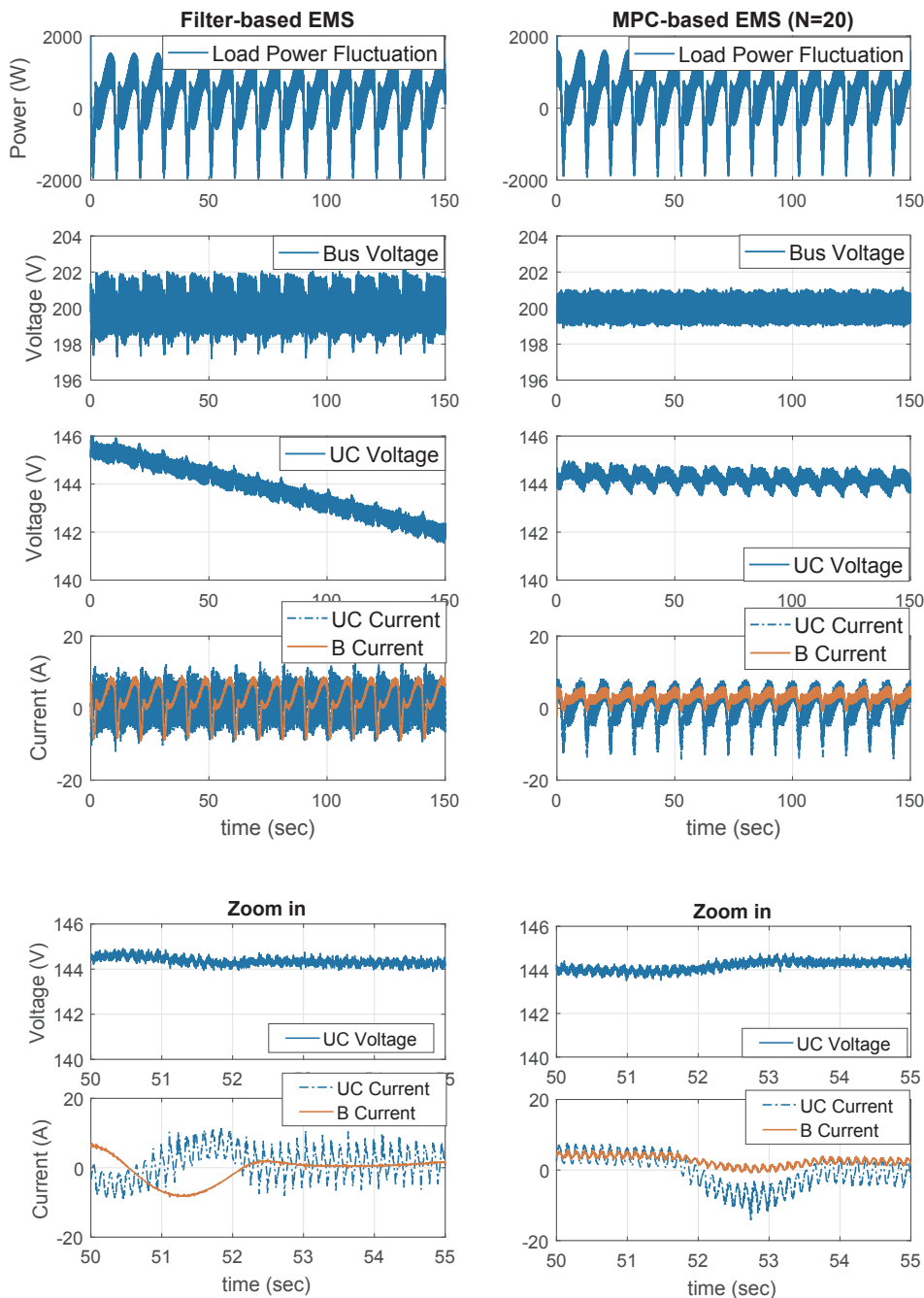
Fig. 19. Experimental results of sea state 6: MPC vs. filter-based control.

generator sets, the second DC/DC converter (PCM2) is controlled to provide the average current for the DC bus. Since the bus voltage is well regulated, the second DC/DC converter (PCM2) is almost provided the average power. PCM3, PCM4 and PCM5 are used to control the power flow of battery, ultracapacitor and resistive load bank, respectively. The resistive load bank is controlled to emulate the propulsion-load fluctuations by using the propulsion-load model and pulse-power loads with about 1 kW amplitude and 1 s duration [47]. The pulse power load is used to demonstrate the effectiveness of the proposed method. The duration of pulse power load is not necessary to be 1 s. The HESS compensates the load fluctuations to maintain a constant DC bus voltage. The predictive horizon is chosen to be N = 20. Note that the scaling factor is based on the resistive load bank, which is capable of providing a peak power of 2 kW. This resistive load bank is a key component to emulate different applications, which include not only

ship applications, but also other applications in automotive and microgrid fields.

4.3. Component-level control validation

As the first step, the performance of component-level controllers is validated in the MPEL AED-HES test-bed. The system micro-controller, made by Speedgoat, supports Matlab Real-Time Simulink to enable rapid prototyping of advanced control algorithms. Specifications for the Speedgoat®system controller are provided in Table 4. A center-based PWM trigger signal enables the synchronization of the PWM waveforms and analog-to-digital measurements. The trigger signal is generated at the center of PWM waveforms. The kernel of Speedgoat receives this trigger signal to read A/D feedback, and then initiates the controller computation. Once the controller computation is completed, PWM
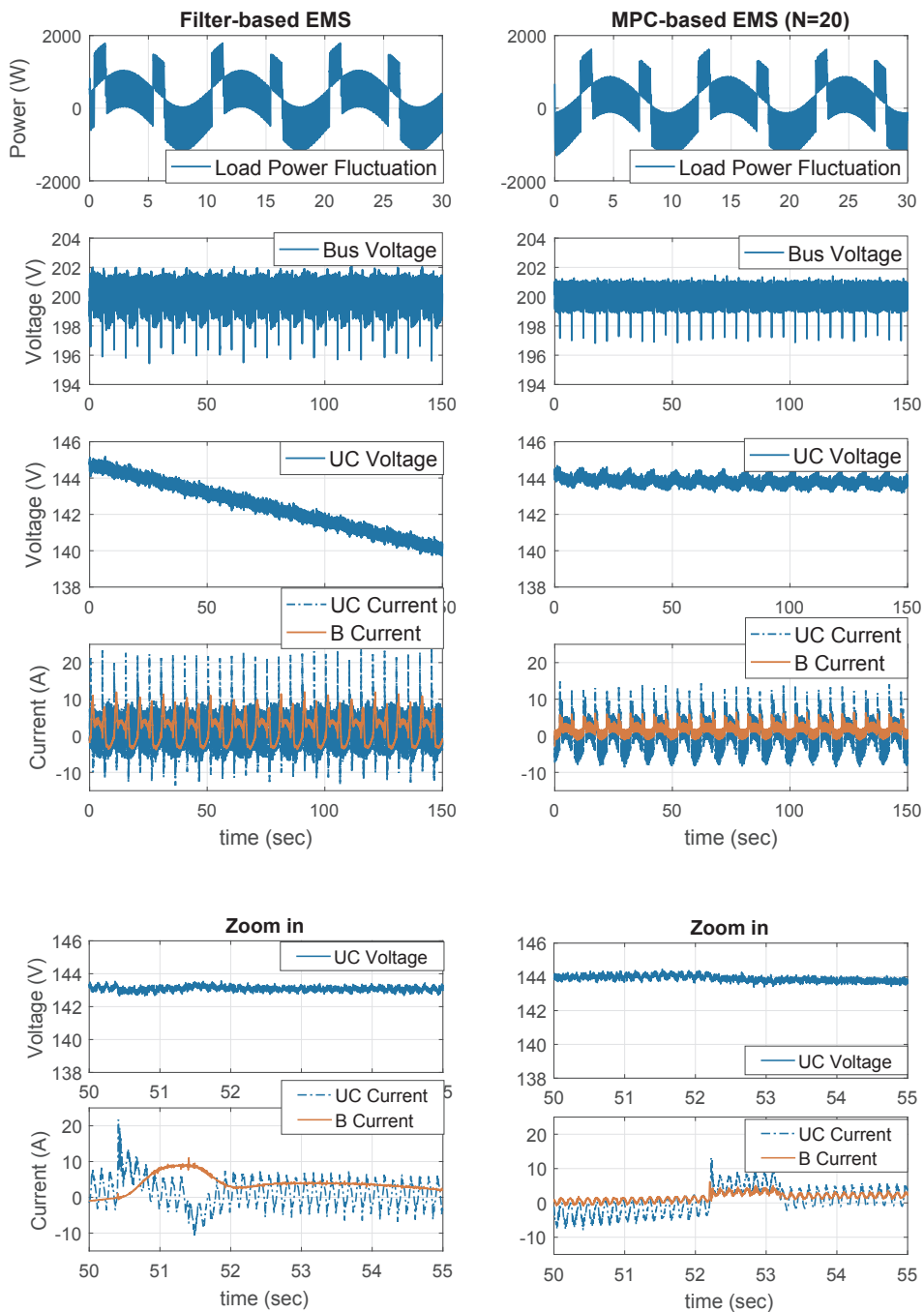
Fig. 20. Experimental results of pulse power load: MPC vs. filter-based control.

counter values, which determine the duty cycles, are updated for the next switching period. This center-based trigger reduces the effects of noise, as the switching of the power electronic transistors and the sampling of the analog-to-digital converters are synchronized. Consequently, sampling always occurs in between switching transitions, avoiding the pick-up of electromagnetic interference caused by the transitions. Center-based sampling is also able to measure the average value of the inductor current. However, due to hardware delays, a phase shift can cause measurement errors which can be significant when the value of the measurement is small. Our double-sampling method, which samples twice within one switching period, can achieve more accurate average feedback. As shown in Fig. 14, the actual output power of the HESS can follow the power reference quite accurately.

4.4. Real-time computational capability validation

The real-time computational capability is validated in the following. In addition to the efficient optimization algorithm described in the previous section, exploiting parallel computing using a multi-core micro-controller structure can also increase the computational capabilities of our system [53,54]. In this experiment, the system-level controller is executed in core 1, while the component-level controllers are executed in core 2. Both system-level and component-level controllers are synchronized with the center-based trigger signal. The multi-core structure in Matlab/Simulink is shown in Fig. 15. The sampling frequency of core 1 is 100 Hz (i.e., MPC), while the sampling frequency of core 2 is 20 kHz. The outputs of core 1 will be the command or reference for core 2. A real-time simulation is performed to

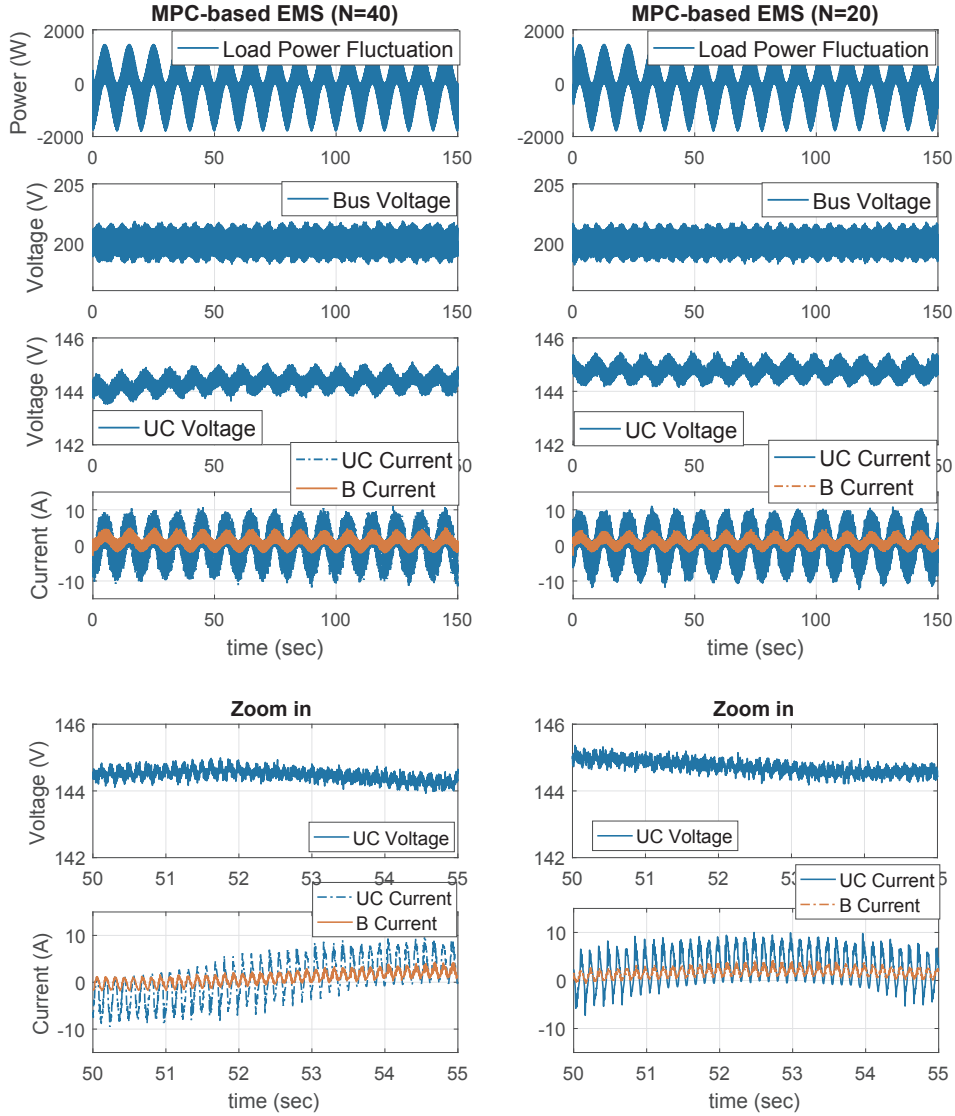
MPC-based EMS (N=40)
MPC-based EMS (N=20)
Power (W)
2000
0
-2000
Load Power Fluctuation
Voltage (V)
205
200
Bus Voltage
146
144
142
UC Voltage
UC Current
B Current
Current (A)
10
0
-10
0
50
100
150
time (sec)
Zoom in
50
51
52
53
54
55

Fig. 21. Experimental results of sea state 4: MPC(N = 20) vs. MPC(N = 40).

evaluate the computational capability of our proposed hierarchical real-time MPC. As shown in Figs. 16 and 17, the maximum execution time for cores 1 and 2 are smaller than their corresponding sampling times. Even though the average and maximum execution times in core 1 are much smaller than its sampling time (0.01 s), it is not feasible to implement the MPC on core 2. It is essential to implement real-time MPC in a multi-core structure.

4.5. Experimental results and discussion

In this experimental study, the internal resistances of battery (R_B) and UC (R_{UC}) are obtained from experimental identification results using the recursive least square. The experimental results of the filter-based and real-time MPC strategies to deal with propulsion-load fluctuations are shown in Figs. 18 (sea state 4) and 19 (sea state 6). The results of the propulsion load fluctuations with pulse power loads are shown in Fig. 20. The following performance metrics (performance improvement) are used to compare the real-time MPC with the filter-based strategy:

1. Voltage variation ($Volt_{var}$): $\frac{rms(Vbus_{baseline}-Vbus_{ref})-rms(Vbus_{testing}-Vbus_{ref})}{rms(Vbus_{baseline}-Vbus_{ref})}\times$ 100%;
2. Estimated HESS losses ($HESS_{Loss}$): $\frac{Losses_{baseline}-Losses_{testing}}{Losses_{baseline}}\times$ 100%;
3. Battery peak current (B_{Peak}): $\frac{max(|I_{B,baseline}|)-max(|I_{B,testing}|)}{max(|I_{B,baseline}|)}\times$ 100%;
4. Battery RMS current (B_{RMS}): $\frac{rms(I_{B,baseline})-rms(I_{B,testing})}{rms(I_{B,baseline})}\times$ 100%.

In this section, the proposed MPC algorithm is the testing algorithm and the filter-based is the baseline algorithm. As shown in Table 5, compared with the filter-based strategy, the proposed real-time MPC can improve the bus voltage variation 38% of the filter-based approach, and HESS total losses are improved as high as 65% of the filter-based approach. Furthermore, the real-time MPC operates with much smaller battery peak and RMS currents than the filter-based strategy, leading to an extended battery life cycle. As shown in Figs. 18–20, the UC is operating around the desired reference voltage under the real-time MPC strategy in all scenarios, while the voltage of UC keeps decreasing under the filter-based strategy. Although the generator is assumed to provide the average power for the propulsion system, the UC voltage still drops as shown in Figs. 18 and 19. This performance is mainly caused by the HESS losses, undesirable interaction, and the uncertainties. The undesirable interaction between battery and UC can also increase the HESS losses. The decreasing rate of UC voltage under pulse power loads is higher than those in the other two cases, because the HESS fully compensates the discharge pulses. The efficiency of the filter-based
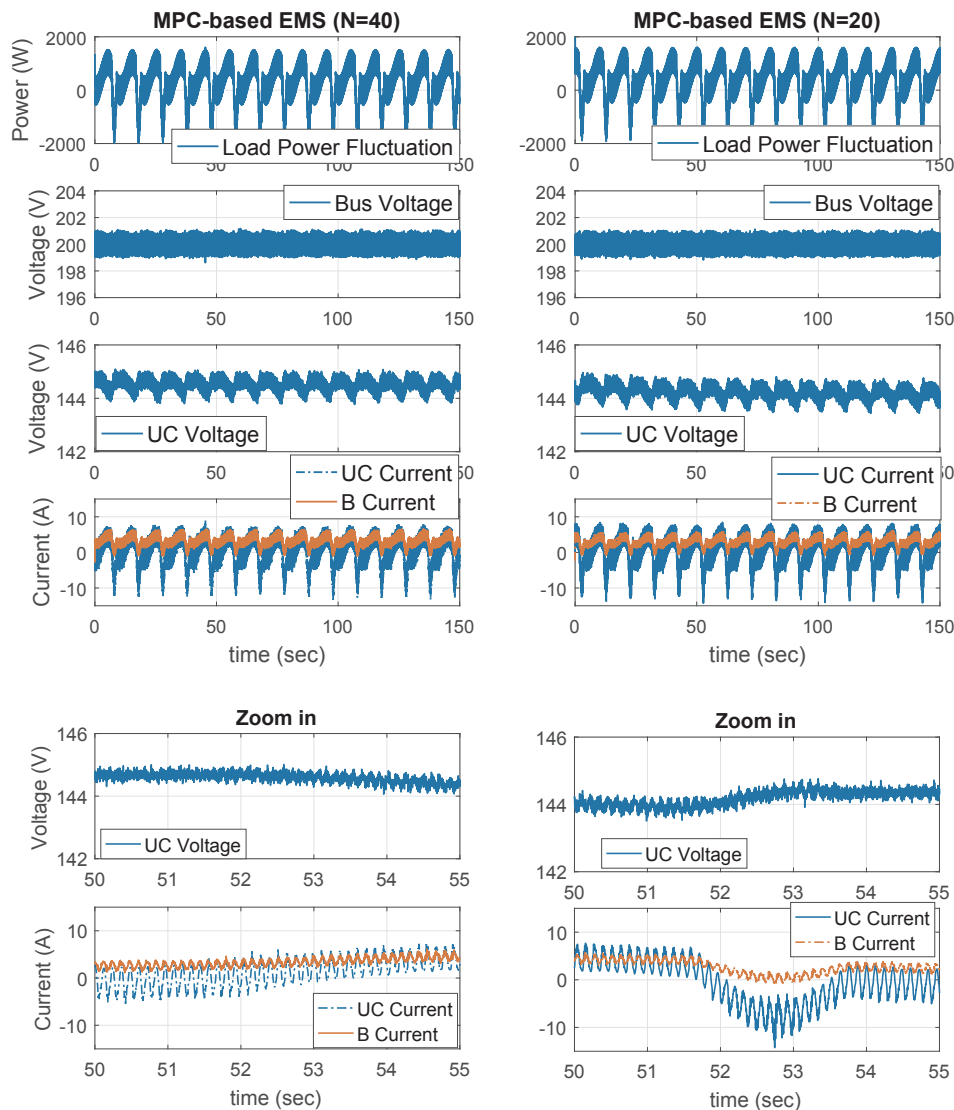
Fig. 22. Experimental results of sea state 6: MPC(N = 20) vs. MPC(N = 40).

strategy will decrease as the UC voltage drops, and so the self-sustained time of the filter-based strategy is much shorter than the real-time MPC. In summary, compared to the baseline control, this experiment shows the effectiveness of the proposed real-time MPC in terms of enhanced system reliability, improved HESS efficiency, long self-sustained time, and extended battery life cycle.

The predictive horizon was found to be an important design parameter. Extending the predictive horizon will generally improve performance at the cost of increased computational complexity. However, when uncertainties exist, performance improvement with increasing horizon is not guaranteed. In order to provide insight into the predictive horizon, the real-time MPC with an extended predictive horizon N = 40 is implemented on the testbed. The experimental results are shown in Figs. 21–23. As shown in these figures, the difference between MPC(N = 20) and MPC(N = 40) is not obvious, especially in Fig. 23. In order to compare these two predictive horizons, the numerical results are required. In this case, MPC(N = 20) is the baseline algorithm and MPC(N = 40) is the testing algorithm.

As shown in Table 6, MPC with N = 40 does not outperform MPC with N = 20 in most performance metrics. The real-time MPC only applies the first element of the control sequence as the control action before moving to the next sample, when new measurements are collected and the optimization is repeated with new initial conditions. This

feedback mechanism is helpful to improve the robustness of the MPC strategy. However, as the predictive horizon increases, it is seen that uncertainties can affect the control performance more significantly than a short predictive horizon. In this study, therefore, the predictive horizon was chosen to be N = 20.

As presented in the literature, MPC has been found to be a robust type of control in many applications, although the stability and robustness proofs are difficult [55]. Furthermore, the bus voltage regulation is combined with MPC to deal with uncertainties. Parameter uncertainties exist in every element, such as battery, ultracapacitors and power electric converters. The predictive uncertainties include two parts: one is from the predictive method; another is caused by the resistance uncertainty of the resistive load bank, since the resistance is changed as its temperature increases. Uncertainties discussed above are useful to evaluate the effectiveness of the control algorithm. Therefore, the experimental results demonstrate the robustness of the proposed control system, given predictive errors, parameter uncertainties and unmodeled dynamics (model simplification).

5. Conclusion

This paper aims to address shipboard load fluctuations, including not only propulsion-load fluctuations but also pulse-power loads, and
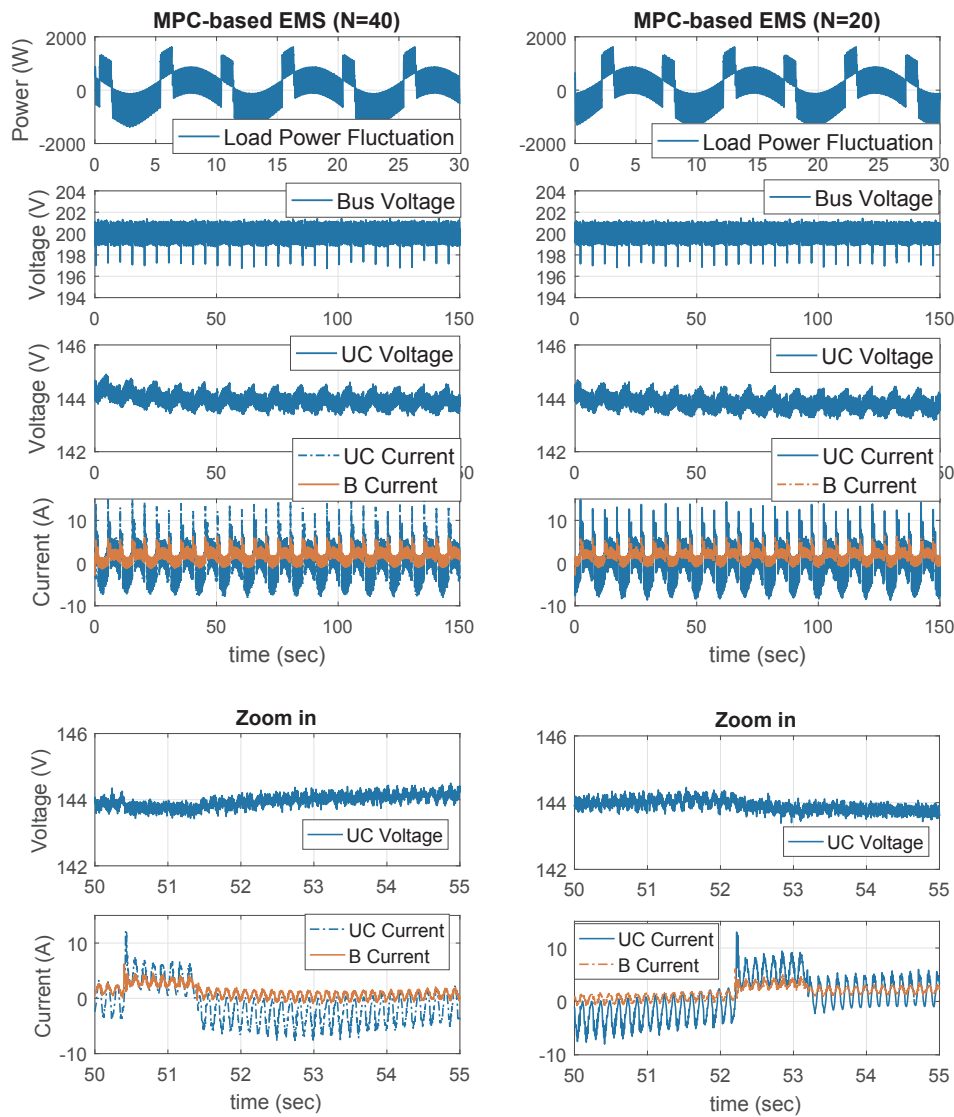
Fig. 23. Experimental results of pulse power load: MPC(N = 20) vs. MPC(N = 40).

Table 6
Performance comparison: MPC(N = 20) vs. MPC(N = 40).

	SS4	SS6	SS4 with pulse
$Volt_{var}$	−2.27%	−0.52%	−1.45%
$HESS_{Loss}$	−1.86%	−10.59%	1.45%
B_{Peak}	−7.69%	−7.67%	1.70%
B_{RMS}	−5.94%	−8.36%	−0.44%

validate the effectiveness of MPC on a physical testbed. The HESS is used as a buffer to isolate the load fluctuations on the shipboard network, and the real-time MPC-based EMS is developed to achieve enhanced system reliability and improved system efficiency. This real-time MPC is implemented and evaluated in the testbed, which is used to emulate the load fluctuations. Compared to the filter-based power split strategy, the proposed MPC-based EMS is demonstrated on the testbed to have superior performance in terms of reduced bus voltage variation, battery peak and RMS currents, and HESS losses. The bus voltage variation and hybrid energy storage losses can be reduced by up to 38% and 65%, respectively. Given the uncertainties associated with the problem and hardware setup, the robustness of the proposed MPC is also validated. The proposed method could deal with more general load fluctuation problems, such as load fluctuations in electric vehicles or

shore-based microgrids.

The main contribution of this paper is to achieve real-time feasibility of MPC-based EMS. Three specific efforts have been made: properly formulating the optimization problem, identifying an efficient optimization solver, and implementing the controller with a multi-core structure. The proper formulation includes both the cost function formulation and system dynamics simplification. Note that the choice of the solver highly depends on the optimization problem, and therefore IPA-SQP is used herein to solve the optimization problem efficiently. The implementation of MPC-based EMS is also important. The multi-core structure can guarantee system signal synchronization and separate system-level and component-level controls. In the future work, we will study the generalization of the proposed algorithm for other potential applications (such as electric vehicles, microgrids, and electric trains) and investigate in what conditions the hybrid energy storage with the proposed strategy provides significant benefits. Furthermore, the irregular wave model for shipboard microgrids will particularly be one of our focuses in the future.

Acknowledgment

thank the editor and reviewers for their valuable feedback.

References

[1] Zhu JY, Chen L, Wang B, Xia LJ. Optimal design of a hybrid electric propulsive system for an anchor handling tug supply vessel. Appl Energy 2018;226:423–36.

[2] Geertsma RD, Negenborn RR, Visser K, Loonstijn MA, Hopman JJ. Pitch control for ships with diesel mechanical and hybrid propulsion: modelling, validation and performance quantification. Appl Energy 2017;206:1609–31.

[3] Balsamo F, Capasso C, Miccione G, Veneri O. Hybrid storage system control strategy for all-electric powered ships. Energy Procedia 2017;126:1083–90.

[4] Skjong E, Volden R, Rødskar E, Molinas M, Johansen T, Cunningham J. Past, present, and future challenges of the marine vessel's electrical power system. IEEE Trans Transport Electrif 2016;2(4):522–37.

[5] Zahedi B, Norum LE, Ludvigsen KB. Optimized efficiency of all-electric ships by dc hybrid power systems. J Power Sources 2014;255:341–54.

[6] McCoy Timothy J. Electric ships past, present, and future [technology leaders]. IEEE Electrif Mag 2015;3(2):4–11.

[7] Doerry Norbert. Naval power systems: integrated power systems for the continuity of the electrical power supply. IEEE Electrif Mag 2015;3(2):12–21.

[8] Hou J, Sun J, Hofmann HF. Control development and performance evaluation for battery/flywheel hybrid energy storage solutions to mitigate load fluctuations in all-electric ship propulsion systems. Appl Energy 2018;212:919–30.

[9] McCoy Timothy J. Integrated power systems-an outline of requirements and functionalities for ships. Proc IEEE 2015;103(12):2276–84.

[10] Hebner RE, Davey K, Herbst J, Hall D, Hahne J, Surls DD, et al. Dynamic load and storage integration. Proc IEEE 2015;103(12):2344–54.

[11] Zhang S, Xiong R. Adaptive energy management of a plug-in hybrid electric vehicle based on driving pattern recognition and dynamic programming. Appl Energy 2015;155:68–78.

[12] Zhang S, Xiong R, Cao J. Battery durability and longevity based power management for plug-in hybrid electric vehicle with hybrid energy storage system. Appl Energy 2016;179:316–28.

[13] Song Z, Hofmann H, Li J, Hou J, Han X, Ouyang M. Energy management strategies comparison for electric vehicles with hybrid energy storage system. Appl Energy 2014;134:321–31.

[14] Song Z, Hofmann H, Li J, Hou J, Zhang X, Ouyang M. The optimization of a hybrid energy storage system at subzero temperatures: energy management strategy design and battery heating requirement analysis. Appl Energy 2015;159:576–88.

[15] Veneri O, Capasso C, Patalano S. Experimental investigation into the effectiveness of a super-capacitor based hybrid energy storage system for urban commercial vehicles. Appl Energy [in press]. Available: https://doi.org/10.1016/j.apenergy.2017.08.086.

[16] Hou J, Sun J, Hofmann HF. Mitigating power fluctuations in electric ship propulsion with hybrid energy storage system: design and analysis. IEEE J Ocean Eng 2018;43(1):93–107.

[17] Capasso C, Veneri O. Experimental analysis on the performance of lithium based batteries for road full electric and hybrid vehicles. Appl Energy 2014;136:921–30.

[18] Sun Jing. Optimisation-based control for electrified vehicles: challenges and opportunities. J Control Decis 2015;2(1):46–63.

[19] Kuseian John. Naval power systems technology development roadmap. Electric Ships Office, PMS, 320; 2013.

[20] Mayne DQ. Model predictive control: recent developments and future promise. Automatica 2014;50(12):2967–86.

[21] Qin S, Badgwell TA. A survey of industrial model predictive control technology. Control Eng Pract 2003;11(7):733–64.

[22] Zia MF, Elbouchikhi E, Benbouzid M. Microgrids energy management systems: a critical review on methods, solutions, and prospects. Appl Energy 2018;222:1033–55.

[23] Geertsma RD, Negenborn RR, Visser K, Hopman JJ. Design and control of hybrid power and propulsion systems for smart ships: a review of development. Appl Energy 2017;194:30–54.

[24] Zhang S, Xiong R, Sun F. Model predictive control for power management in a plug-in hybrid electric vehicle with a hybrid energy storage system. Appl Energy 2017;185:1654–62.

[25] Arce A, Alejandro J, Bordons C, Ramirez D. Real-time implementation of a constrained MPC for efficient airflow control in a PEM fuel cell. IEEE Trans Ind Electron 2010;57:1892–905.

[26] Ghoumari ME, Tantau HJ, Serrano J. Non-linear constrained MPC: real-time implementation of greenhouse air temperature control. Comput Electron Agric 2005;49:345–56.

[27] Böck M, Kugi A. Real-time nonlinear model predictive path-following control of a laboratory tower crane. IEEE Trans Control Syst Technol 2014;22:1461–73.

[28] Ingebrigtsen Bø Torstein. Scenario-and optimization-based control of marine electric power systems [PhD thesis]. Trondheim, Norway: NTNU; 2016.

[29] Park H, Sun J, Pekarek S, Stone P, Opila D, Meyer R, et al. Real-time model predictive control for shipboard power management using the ipa-sqp approach. IEEE Trans Control Syst Technol 2015;23(6):2129–43.

[30] Seenumani G, Sun J, Peng H. Real-time power management of integrated power systems in all electric ships leveraging multi time scale property. IEEE Trans Control Syst Technol 2012;20(1):232–40.

[31] Ingebrigtsen Bø Torstein, Arne Johansen Tor. Battery power smoothing control in a marine electric power plant using nonlinear model predictive control. IEEE Trans Control Syst Technol 2017;25(4):1449–56.

[32] Ingebrigtsen Bø Torstein, Arne Johansen Tor. Dynamic safety constraints by scenario-based economic model predictive control of marine electric power plants. IEEE Trans Transp Electrif 2017;3(1):13–21.

[33] Haseltalab A, Negenborn RR, Lodewijks G. Multi-level predictive control for energy management of hybrid ships in the presence of uncertainty and environmental disturbances. IFAC-PapersOnLine 2016;49(3):90–5.

[34] Park H, Sun J, Kolmanovsky I. A tutorial overview of ipa-sqp approach for optimization of constrained nonlinear systems. In: 2014 11th world congress on intelligent control and automation (WCICA). IEEE; 2014. p. 1735–40.

[35] Ghaemi R, Sun J, Kolmanovsky I. An integrated perturbation analysis and sequential quadratic programming approach for model predictive control. Automatica 2009;45(10):2412–8.

[36] Bryson A, Ho Y. Applied optimal control: optimization, estimation, and control. Taylor & Francis; 1975.

[37] Ghaemi R. Robust model based control of constrained systems [Ph.D. thesis]. The University of Michigan; 2010.

[38] Cupelli M, Ponci F, Sulligoi G, Vicenzutti A, S Edrington C, El-Mezyani T, et al. Power flow control and network stability in an all-electric ship. Proc IEEE 2015;103(12):2355–80.

[39] Yan D, Lu L, Li Z, Feng X, Ouyang MG, Jiang F. Durability comparison of four different types of high-power batteries in hev and their degradation mechanism analysis. Appl Energy 2016;179:1123–30.

[40] Omar N, Monem M, Firouz Y, Salminen J, Smekens J, Hegazy O, et al. Lithium iron phosphate based battery-assessment of the aging parameters and development of cycle life model. Appl Energy 2014;113:1575–85.

[41] Masih-Tehrani M, Ha'iri-Yazdi M, Esfahanian V, Safaei A. Optimum sizing and optimum energy management of a hybrid energy storage system for lithium battery life improvement. J Power Sources 2013;244:2–10.

[42] Hu X, Li S, Peng H. A comparative study of equivalent circuit models for Li-ion batteries. J Power Sources 2012;198:359–67.

[43] Song Z, Li J, Han X, Xu L, Lu L, Ouyang M, et al. Multi-objective optimization of a semi-active battery/supercapacitor energy storage system for electric vehicles. Appl Energy 2014;135:212–24.

[44] Liang J, Qi L, Lindtjørn J, Frank Wendt. Frequency dependent DC voltage droop control for hybrid energy storage in DC microgrids. In: 2015 IEEE power & energy society general meeting; 2015. p. 1–5.

[45] Zahedi B, Norum LE. Modeling and simulation of all-electric ships with low-voltage DC hybrid power systems. IEEE Trans Power Electron 2013:4525–37.

[46] Hou J, Reed DM, Hofmann H, Sun J. A low-voltage test-bed for development and validation of control strategies for electric propulsion systems with hybrid energy storage. Naval Eng J 2017.

[47] Park Hyeongjun. Real-time predictive control of constrained nonlinear systems using the ipa-sqp approach [Ph.D. thesis]. The University of Michigan; 2014.

[48] Slotine J, Li W, et al. Applied nonlinear control vol. 199. NJ: Prentice hall Englewood Cliffs; 1991.

[49] Song Z, Hou J, Hofmann H, Li J, Ouyang MG. Sliding-mode and Lyapunov function-based control for battery/supercapacitor hybrid energy storage system used in electric vehicles. Energy 2017;122:601–12.

[50] Gulev SK, Hasse L. North Atlantic wind waves and wind stress fields from voluntary observing ship data. J Phys Oceanogr 1998;28:1107–30.

[51] Smogeli ØN, Sørensen AJ. Antispin thruster control for ships. IEEE Trans Control Syst Technol 2009;17(6):1362–75.

[52] Hou J, Sun J, Hofmann HF. Adaptive model predictive control with propulsion load estimation and prediction for all-electric ship energy management. Energy 2018;150:877–99.

[53] Luszczek Piotr. Enhancing multicore system performance using parallel computing with matlab. MATLAB Digest 2008;17(5).

[54] Kepner Jeremy. Parallel MATLAB for multicore and multinode computers. SIAM; 2009.

[55] Camacho EF, Bordons C. Model predictive control, 2nd ed.; 2013.